

Low-temperature infrared properties of cosmic dust analogues

Th. Henning and H. Mutschke

Astrophysical Institute and University Observatory, Schillergäßchen 2-3, D-07745 Jena, Germany

Received 13 January 1997 / Accepted 27 June 1997

Abstract. Cosmic dust analogue materials including amorphous and crystalline silicates, ferrous oxide, and iron sulfide have been studied by reflectance spectroscopy of bulk surfaces as well as by transmission spectroscopy of particulates at temperatures down to 10 K. From the reflectance measurements optical data have been derived. The spectra show a sharpening and strengthening of the vibrational bands with decreasing temperature. This effect is weak for the silicates, surprisingly also for the crystalline one, with the exception of the far-infrared metal ion vibrations found in a pyroxene glass of approximately cosmic composition. For the iron compounds, the strengthening of the bands is considerably stronger. The FIR continuum absorption caused by free charge carriers in the semiconducting materials and by phonon difference processes in the crystalline silicate, respectively, decreased with decreasing temperature as expected. Part of the temperature effects are masked in the transmission spectra by the complicated particle morphology.

Key words: interstellar medium: dust, extinction – infrared: ISM: continuum – infrared: ISM: lines and bands

1. Introduction

For a long time, it has been argued that the optical properties of cosmic dust particles at the low temperatures of the dense interstellar medium phases are different from those at room temperatures (see, e.g., Day 1976). If true, this would be of considerable astrophysical importance since the wavelength-dependent emission cross sections of these particles are critical parameters in the determination of the total dust masses of molecular cloud cores, proto-planetary accretion disks, and galaxies from their thermal dust radiation (Henning et al. 1995a).

From solid-state physics, it is clear that a variety of reasons, such as phase transitions, changes of the phonon and of the free charge carrier populations, may influence the optical behaviour of a solid if it is cooled down to temperatures of several 10 K. These effects should be especially strong at far-infrared

(FIR) wavelengths where the photon-induced transitions compete with thermal excitation. Therefore, most experiments investigating the optical properties of solids at low temperatures have been carried out in the infrared region. Measurements already performed in the sixties concerned the lattice vibration bands of crystalline dielectrics such as halides including the phonon difference processes occurring in the FIR (Jasperse et al. 1966; Stolen & Dransfeld 1965; Hadni 1970, see also Sect. 2.1). In the seventies, the field of interest shifted to low-energy transitions occurring in amorphous semiconductors and silicate glasses (Mon et al. 1975; Strom & Taylor 1977; Bösch 1978). These transitions dominating the absorption in amorphous silicates in the submm- and mm-region are also of great interest for the emission of cold interstellar dust (Agladze et al. 1994, 1996).

Despite these investigations, detailed studies on the low-temperature optical behaviour of most of the materials relevant for astrophysics are still lacking and optical data are not available. With this paper, we try to reduce this gap by measuring the low-temperature infrared spectra of some of our previously studied dust analogue materials which are an amorphous silicate of pyroxene stoichiometry with a cosmic composition of the metals (Jäger et al. 1994), ferrous oxide (FeO) (Henning et al. 1995b), and iron sulfide (Begemann et al. 1994). We added a crystalline silicate of pyroxene type (bronzite) spectroscopically analyzed by Dorschner et al. (1988) to this list, since such a material seems to become important for the interpretation of ISO spectra (Waters et al. 1996). Moreover, we analyzed the low-temperature spectroscopic behaviour of amorphous SiO₂ (quartz glass) which is of principal interest as the most ideal amorphous silicate.

Referring to our intention to provide the optical constants (complex refractive index $m = n + ik$, or dielectric function $\varepsilon = m^2$), we performed specular reflectance spectroscopy which avoids the uncertainties arising from the geometry of particle samples. The spectra have been measured in the 2–500 μm wavelength range corresponding to wavenumbers (reciprocal wavelength) between 5000 and 20 cm^{-1} . The results of the reflection measurements are given in Sect. 4.

The reflectance, however, is not expected to yield sufficient information about small continuum absorption in the far infrared. To improve this situation, we also measured transmittance spectra of fine powders diluted in KBr and polyethylene

(PE) and compared them to theoretical ones calculated from the optical constants (Sect. 5). Before discussing the results, we give a short introduction to the temperature effects which are expected in the spectra of cosmic dust analogues (Sect. 2). The experimental details are described in Sect. 3.

2. Temperature effects in the infrared spectra of insulators and semiconductors

Cosmic dust is expected to contain a large variety of materials. The main components should be silicates, carbon modifications, and ices but other oxides, sulfides, and carbides as well as pure metals could also play an important role. These materials cover a wide range of optical properties which are mainly determined by the absorption processes that may occur in the electronic system on the one hand and in the lattice on the other hand. In the infrared spectral range, the dominating absorption processes are phonon (lattice excitation) and free-electron processes. The latter, of course, are only present in conducting (metals) and semiconducting materials which in space are mainly represented by carbon, silicon carbide, and iron compounds (e.g., FeO and FeS). Carbon soot particles are a very special case due to their complicated structure and microtexture (Jäger 1997) and will be the subject of another paper.

2.1. Phonon processes

Lattice vibration modes in an ideal *crystal* can be excited by electromagnetic radiation if they are connected to the oscillation of an electrical dipole (optical modes) and, further, if energy and momentum are conserved. Because of the momentum condition, single phonons can only be created if their wavenumber is comparable to that of the IR radiation. The corresponding very prominent absorption bands (reststrahlen bands) usually dominate the optical behaviour of a dielectric heteroatomic material in the infrared range.

In addition to the single phonon excitation, multiphonon processes contribute to the IR absorption but with a far less probability. In these processes, any combination of acoustic, optical, transverse, and longitudinal phonons can take part, which satisfies the energy and momentum conditions. Multiphonon processes are a main source of infrared absorption in homoatomic solids as diamond, silicon etc.. Furthermore, they dominate the absorptivity of dielectric ionic crystals in the infrared outside the reststrahlen bands. Especially at long wavelengths, phonon difference processes (one phonon is created, one of lower energy destroyed) are responsible for the absorptivity of ionic crystals. As the probability of these processes depends on the density of the phonons which are to be destroyed, the far-infrared absorptivity of these crystals decreases drastically with the freezing of lattice vibrations at decreasing temperatures (Hadni 1970).

For the single-phonon absorption, temperature effects should be less significant because the occurrence of an absorption process does not depend on the excitation state of the material. However, in the case of thermal excitation, further transitions caused by infrared illumination may occur between higher vi-

brational states. Because of the anharmonicity of the potential, the resonance frequency of these transitions is slightly shifted. Consequently, the absorption band of a warm solid is shifted to lower frequencies and broadened with respect to a colder one.

Special attention has to be given to the behaviour of *amorphous materials*. Their presence in space is evident because many interstellar emission and absorption bands are very broad and featureless. Disorder of the atomic arrangement leads to a break-down of the selection rules for the wavenumber and the possibility to excite all vibrational modes directly by single-mode processes. Thus, absorption spectra of amorphous materials reflect the whole density of vibrational states which is itself smeared out compared to crystalline materials due to the statistical variation in bond length and angle. Consequently, the phonon absorption bands are much broader than those of their crystalline counterparts. Towards longer wavelengths, a continuous absorption due to the disorder-induced single-mode processes completely dominates over the multiphonon absorption. Since the temperature dependence of the single-phonon absorption is only weak, the FIR absorption at low temperatures does not vanish for amorphous solids in contrast to the crystalline ones.

2.2. Free-electron excitation

For the free electrons, one has to distinguish between metals in which they are permanently present and semiconductors where they are produced by thermal excitation of donor or valence electrons to the conduction band. For metals, therefore, the number of free electrons is temperature-independent and of the same order of magnitude as the number of atoms. In contrast to this, for semiconductors the number of free charge carriers roughly follows a Boltzmann law with the corresponding energy difference (band gap) as the parameter. Restricting ourselves to undoped semiconductors, we find that about 10^{21} free charge carriers per m^3 are available at room temperature in a semiconductor with a low band gap of about 0.5 eV. The plasma frequency ω_p of this free-electron gas is of the order of 10^{12} s^{-1} corresponding to the frequency of electromagnetic radiation in the sub-mm wavelength range. Already a cooling to 100 K, however, results in a decrease of the number of charge carriers down to 10^{11} m^{-3} . This causes a shift of the plasma edge to a wavelength of many metres and should change completely the measured spectrum of such a material. Compared to semiconductors, the number of electrons in a metal is by several orders of magnitude higher, which corresponds to a plasma frequency in the ultraviolet.

The optical effects in bulk samples resulting from the free charge carriers are first a high reflectivity (“plasma reflection”) at wavelengths upwards and second decreasing absorbance at wavelengths downwards from the plasma resonance. For small particles, the most significant effect of free charge carriers is the occurrence of plasma resonances (surface plasmons) at wavelengths larger than $\lambda_p = 2\pi c/\omega_p$ where the real part of the dielectric function is negative. For a spherical particle which is small compared to the wavelength there is one single resonance

and the absorption decreases quadratically to both larger and smaller wavelengths (Seki & Yamamoto 1980).

The positions of these features mainly depend on the concentration of the charge carriers as described above. Therefore, in first approximation they are not temperature-dependent for metals. The exact shape of the dielectric function, however, is also determined by the charge carrier mobility. For a low mobility, for instance, the onset of the plasma reflection can be considerably smeared out. In strong contrast to this, for a low-band-gap semiconductor all the features discussed will shift to larger wavelengths if the material is cooled down and are completely frozen out at very low temperatures.

3. Experiments

3.1. Cryostat

The spectroscopic measurements have been performed with a Bruker 113v Fourier Transform Infrared Spectrometer covering the spectral range from 2 to 500 μm (5000–20 cm^{-1}). A continuous-flow liquid helium cryostat (Cryovac) equipped with KRS5 and polyethylene infrared optical windows (diameter 40 mm) has been adapted to the sample compartment of the spectrometer. In the cryostat, the samples are cooled via helium contact gas (1–5 mbar) which ensures a uniform temperature of the samples but requires a closed sample chamber (diameter 30 mm) inside the cryostat vacuum with additional *cold* windows (diameter 25 mm). Both the temperatures of the liquid helium cooled walls of the sample chamber and of the sample have been measured by means of Si-diode temperature detectors. Spectra have been recorded generally at temperatures of 300, 200, 100, and 10 K. The sample holder is able to keep two samples, thus allowing to switch between the sample and the reference without warming up.

3.2. Materials

The pyroxene glass of “cosmic composition”, the FeO, and the FeS sample have been prepared by melting in an arc furnace and subsequent quenching on a water-cooled copper plate. For the latter two, the preparational details and the results of chemical and structural analytics are described in previous papers (Henning et al. 1995b; Begemann et al. 1994) and will not be repeated here. In the case of the pyroxene glass, we left the preparational path described in our previous papers (Jäger et al. 1994; Dorschner et al. 1995) because the slab-shaped samples prepared in that work led to problems in the spectra evaluation due to the occurrence of multiple reflection. Instead of this, we found that the arc-melting method applied to a natural hypersthene mineral (Paul’s Island, Labrador, Canada) was also able to deliver an amorphous material, at least in a sufficiently thick surface layer in the immediate vicinity of the copper plate (Dorschner et al. 1989). As the back side of the sample remains spherical in this case, radiation reflected at the back side is scattered and does not reach the detector. The cationic composition of the resulting glass in at.%, as determined by energy-dispersive X-ray analysis (EDX), is very similar to that of sample 2 in Jäger

et al. (1994) and closely resembles the cosmic elemental abundances of the metal ions Mg, Fe, Ca, and Al. The abundances are: Mg 28.1%, Fe 17.3%, Al 1.1%, Ca 2.2% and Si 51.3%.

The crystalline bronzite sample (Paterlestein, Franken, Germany) has a much lower iron content than the glassy pyroxene (about 5%) and is polycrystalline with crystallite sizes of about 1 μm . Since the spot size of the spectrometer beam is about 5 mm in diameter, crystallites of different orientation contribute to the reflection signal. In a first approximation, we assume that the different orientations are equally averaged as it is the case in powder samples.

The amorphous SiO_2 sample is a commercial quartz glass window (Suprasil) which has been cut into wedge shape in order to avoid reflection from the back side.

3.3. Sample preparation

For the reflection measurements, all samples except the quartz glass have been embedded into epoxy resin for a better handling and were polished to prepare a smooth and flat surface for the reflection spectroscopy.

For the transmission measurements, the material was ground in a ball mill. The absorption of small particles is independent of the grain size if their characteristic dimensions are much smaller than the wavelength. Therefore, we separated the powder fraction smaller than one micron in diameter by sedimentation in acetone. This fraction was embedded in KBr and PE pellets of 13 mm diameter and 200 mg weight with mass concentrations ranging between 10^{-3} and 10^{-2} . For the amorphous SiO_2 sample, instead of ground material, we used a commercially available powder consisting of mono-sized spherical particles of 500 nm diameter (“Monosphere powder” M 500, MERCK, Darmstadt).

4. Reflection measurements and derivation of optical data

For measuring the specular reflectance of polished sample surfaces, we fitted the cryostat to the standard reflectance accessory of the spectrometer (for quasi-normal incidence of radiation). In this case, the radiation passes two times the same windows of the cryostat. Reflection at the windows leads to an additional signal which can be measured by turning the sample out of the beam. This “zero signal” has to be subtracted both from the measured sample and reference spectra. As the reference, we used a gold-coated mirror the reflectance of which can be considered to be unity in the spectral range of interest.

The resulting reflectance spectra of the samples at the different temperatures are shown in Fig. 1a,b. In order to show more details of the vibrational bands and the FIR region, we omit the wavenumbers larger than 1500 or 1000 cm^{-1} where the reflectivity of the samples is more or less constant. The relative errors of the individual spectra due to uncertainties in the reproducibility of the sample and reference positions and due to the influence of non-vanishing surface curvature and deformation by thermal stress in the sample were estimated to be about $\pm 0.5\%$ in the middle IR and about $\pm 1\%$ in the far IR where a

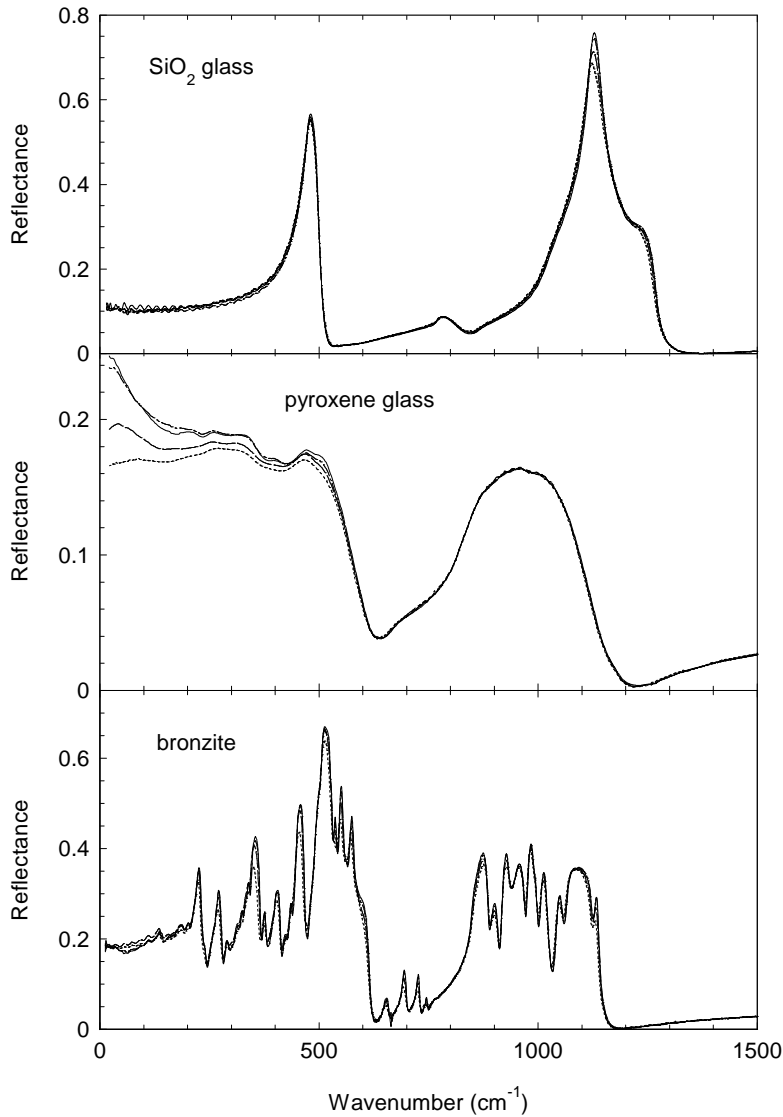


Fig. 1a. Reflectance spectra of silicates at sample temperatures of 300 K (dotted lines), 200 K (dashed lines), 100 K (dash-dotted lines), and 10 K (solid lines).

Si-bolometer detector has been used. With small corrections to the FIR spectra within these errors, the spectra measured with different detectors in the different spectral regions overlap very well.

By comparison with spectra recorded without the cryo-setup, we found (independently of the temperature) a systematic lowering of the reflectance values for the FeO sample (deviations up to -10% of the actual value). This was obviously caused by a too small sample compared with the spot of the spectrometer beam. Since the size of the beam is wavelength-dependent, it was necessary to calculate a wavelength-dependent instrumental function and to multiply all spectra of this sample with this function.

As features in the reflectance spectra indicate only the larger variations of the complex refractive index, the spectra of Fig. 1b show mainly the temperature dependence of the single-phonon and the free charge carrier (in FeO) excitations. From the spectra of the silicates, it is evident that the temperature dependence of the single-phonon excitations is quite weak as expected (see

Sect. 2.1). One exception is the behaviour of the pyroxene glass (see Fig. 1a) in the very far infrared. In this spectral range, a rise in the reflectance indicating vibrational transitions is observed in many glasses (Gervais et al. 1987). This behaviour is caused by vibrations of network-modifier cations such as calcium or sodium relative to the silicate network.

In the case of our pyroxene glass, the rise in the reflectance is not yet present at room temperature but occurs while cooling down. Calcium should be the main carrier of the feature since aluminum mainly acts as a network former and magnesium and iron vibrations occur in the immediate vicinity of the silicate bending mode at about $20 \mu\text{m}$. The strong temperature dependence of this transition is not very surprising since the environment of the metal ions in the glass is irregular and, thus, a large degree of anharmonicity of the potential is expected.

For the semiconductors (FeO, FeS), the reflectance spectra are not only determined by the single-phonon transitions which show a similar temperature dependence like those in the insulators but mainly by electronic effects. In the FIR, a rise in the

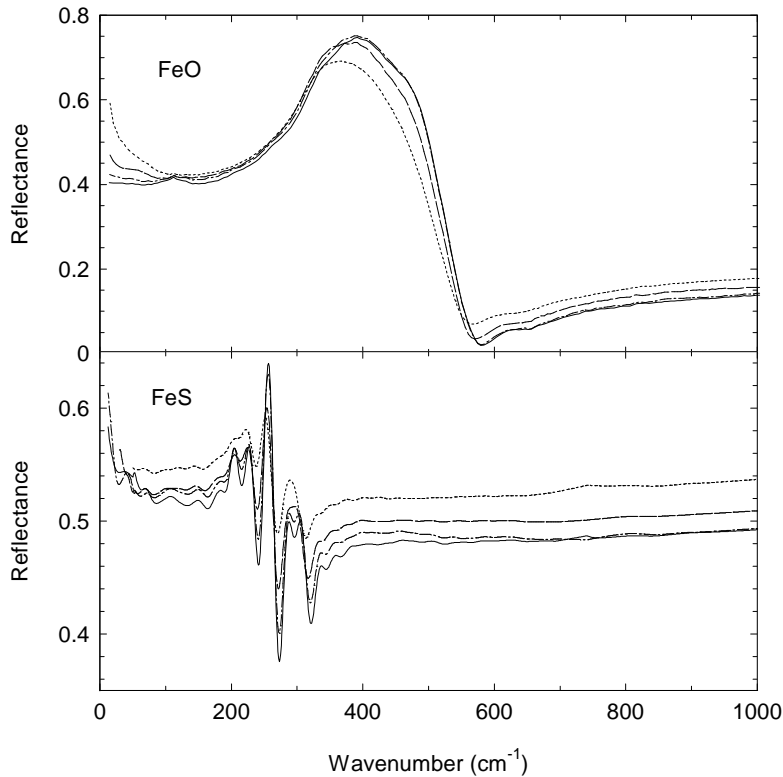


Fig. 1b. Reflectance spectra of iron compounds at sample temperatures of 300 K (dotted lines), 200 K (dashed lines), 100 K (dash-dotted lines), and 10 K (solid lines).

reflectance towards unity occurs which is due to the free charge carriers (see especially the FeO spectrum). As expected, this rise vanishes if the sample is cooled. Even more significant is a decrease in reflectivity in the middle IR which cannot be explained by the free charge carriers. This is very probably an effect of the interband transitions occurring at shorter wavelengths. A thermal shift of the fundamental band gap and changes in the lifetime of excited states are reported in the literature for a number of semiconductors and may be responsible for this behaviour (see, e.g., Yu & Cardona 1996).

From all reflectance spectra, optical data have been calculated by Kramers-Kronig analysis. This procedure requires the choice of convenient extrapolations of the spectra towards zero frequency and for the semiconductors also towards high frequency (in order to abstract from the influence of the interband transitions). The physical consistency of the extrapolations was checked by a sum rule (Harbecke 1986) and by visual inspection of $\text{Im}(\epsilon)$ which never should become negative. For the silicates, this constraint could only be fulfilled by adding an unmeasurably small constant value to the spectrum, since it is crucial that the very small reflectance shortward from the bands has exactly the right value. The resulting optical data are given in Fig. 2a,b. Of course, these n - and k -spectra contain the same information as the reflectance spectra do. However, they show with greater clarity the structure of the absorption bands (in k) and the contributions of the free charge carriers. For the materials without strong absorption in the very far infrared (especially the amorphous SiO_2), it becomes obvious that there is not suffi-

cient information for a correct determination of k in this spectral range.

5. Small particle calculations and transmission measurements

From the optical data derived from the reflection measurements (see the preceding section), it is now possible to calculate the absorption spectra of small particles and to compare them with the results of the transmission measurements as well as with astronomically observed spectra. For this comparison and for the discussion of the temperature effects we plot the calculated (from the reflectance data) as well as the measured small particle spectra (transmission measurements) in terms of the absorption efficiency factor Q normalized by the radius a of a sphere of equal volume. In order to emphasize their origin from different kinds of measurements, we will refer to them as the “reflection” and “transmission” spectra, respectively, regardless of the fact that they show neither reflection nor transmission but absorption (or extinction) in both cases.

We want to state already at this point that the absorption band profiles of small-particle spectra depend not only on the optical data of the particles but also on the refractive index of the matrix material and on the particle morphology. The reason for this behaviour is the occurrence of geometrical resonances (sometimes called surface modes) which dominate the absorption if the band strength is large enough to produce negative values of $\text{Re}(\epsilon)$. These resonances are strongly dependent on the grain shape and on the refractive index of the embedding

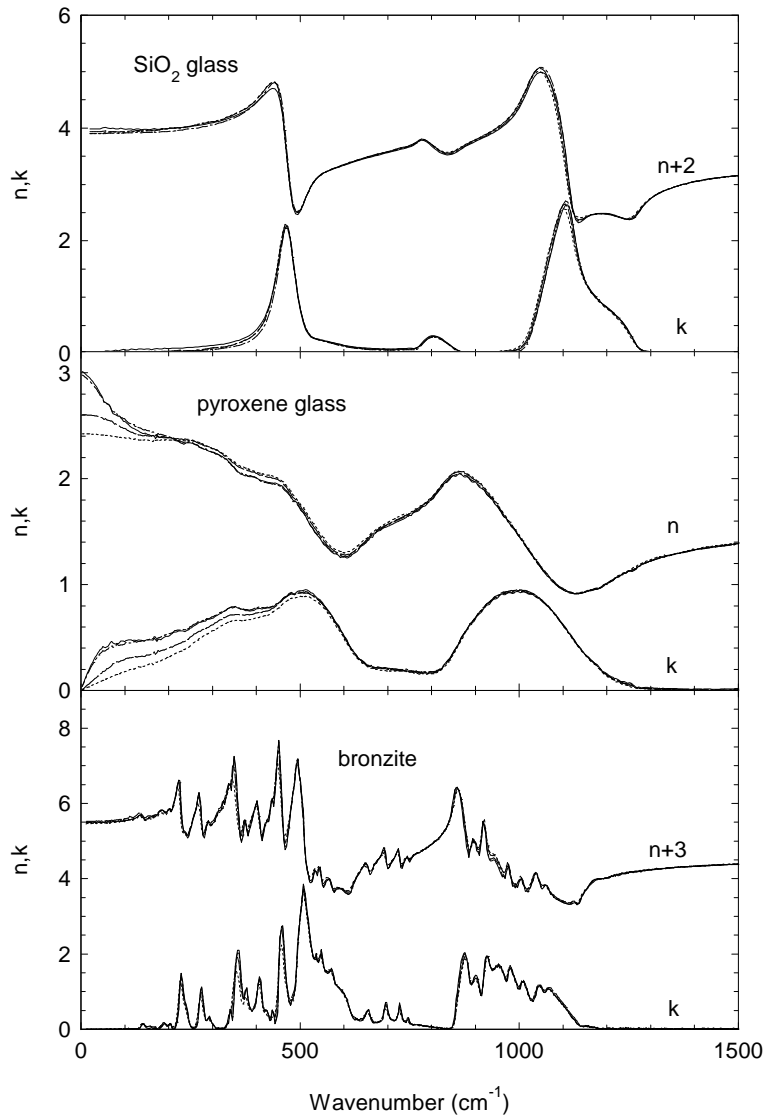


Fig. 2a. Optical data n and k calculated by Kramers-Kronig analysis from the spectra of Fig.1a. Sample temperatures: 300 K (dotted lines), 200 K (dashed lines), 100 K (dash-dotted lines), and 10 K (solid lines).

material which was discussed in previous papers e.g. for silicates (Dorschner et al. 1995) or for FeS (Mutschke et al. 1994).

The transmission spectra have been measured on small particles embedded in KBr (wavenumber range 5000-400 cm^{-1}) and PE (650-20 cm^{-1}). In many cases, the spectra measured in these both ranges did not overlap very well. The reason for this is mainly the poor homogeneity of the PE pellets, which means that the column density varies over the sample area. Deviations up to a factor of two occurred but were easily corrected by multiplying the PE spectrum with a constant factor. In the overlap region, in all cases the KBr values have been used.

Since the far-infrared continuum absorption is of interest by its own, we will discuss it in a separate section and start with the consideration of the single-phonon absorption bands only.

5.1. Single-phonon bands

In Fig.3a,b the calculated absorption spectra (“reflection spectra”) of spherical particles in vacuum are given for the different

temperatures. For all materials except the pyroxene glass, the calculated band profiles show the same thermal behaviour: the bands increase in strength and sharpen with decreasing temperature. For some of them, there is also a small shift towards smaller wavelengths (larger wavenumbers). For the SiO_2 glass as well as for the bronzite, the increase in band strength is of the order of 10%. This is a surprisingly small value for the crystalline silicate. For a crystalline pyroxene (enstatite), Day (1976) reported a much stronger effect, especially in the region of the 20 μm band. For the pyroxene glass, there is no significant temperature dependence in the 10 and 20 μm bands. The FIR transitions of the metal (calcium) ions, however, produce a “quasi-continuum” absorption which obviously dominates the total absorption at wavenumbers smaller than about 450 cm^{-1} and result in an increase of the absorption with falling temperature in this spectral range.

For the iron compounds, the strengthening of the vibrational bands is very significant (factor of 2–3 stronger at 10 K compared to room temperature). However, the reasons for this be-

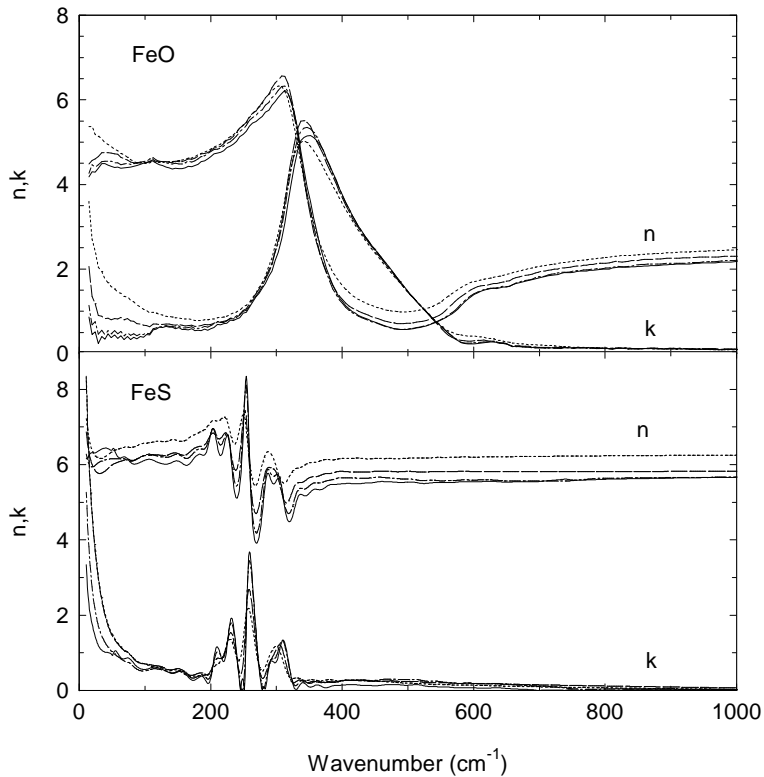


Fig. 2b. Optical data n and k calculated by Kramers-Kronig analysis from the spectra of Fig.1b. Sample temperatures: 300 K (dotted lines), 200 K (dashed lines), 100 K (dash-dotted lines), and 10 K (solid lines).

behaviour are different for FeO and FeS. For the former, the absorption is clearly dominated by a geometrical resonance and occurs at a spectral position (about 450 cm^{-1}) where the real part of the refractive index n is very low. As the “freezing-out” of the free charge carrier absorption leads to a decrease of n with falling temperature, the imaginary part of the dielectric function decreases as well and a weaker damping of the resonance occurs. In contrast to this, for the FeS the strengthening with falling temperature is obviously a consequence of the larger peak values of k and must be considered as an effect of the anharmonicity of the phonon potentials themselves.

The band profiles in the “transmission spectra” (Fig.4) are similar to those in the “reflection spectra” (Fig.3) for the silicates but are significantly different in case of the iron compounds. The reasons for these differences very probably are morphological effects. This means that size, shape or aggregation state of the real particulates embedded in the matrix material deviate from the assumptions of the model (separated spheres in the Rayleigh size limit) that entered into the calculations of the “reflection spectra”. Moreover, the influence of the different matrices (vacuum vs. KBr/PE) has to be taken into account in this comparison but is in all cases not sufficient to explain the differences.

The most striking deviation in the FeS transmission spectra is the occurrence of a huge background absorption increasing towards shorter wavelengths. The phonon bands are small humps on this background, yet invisible at room temperature but rising during the cooling-down of the samples (see Fig.4b). Their strength is comparable to the calculated values. The background can be explained (cf. Begemann et al. 1994) by taking the large

refractive index of the material into account. It leads to a very low Rayleigh limit for the grain size which practically cannot be reached by grinding and sedimentation and, therefore, to the occurrence of scattering and higher-order geometrical resonances in the transmission spectra. This can be illustrated by Mie calculations (Fig.5) which show that already a small admixture of particles in the $1\text{--}2\ \mu\text{m}$ size range is able to produce the steep rise in extinction towards larger wavenumbers that was measured.

For the FeO, the resonance absorption is strongly influenced by shape effects and agglomeration of the grains. This is the reason why the temperature dependence is less significant in the transmission spectra than in the spectra calculated from the reflection data. Such morphological effects have also to be considered for the other materials. Their magnitude can be estimated by calculating the absorption profiles for a continuous distribution of ellipsoidal shapes (CDE) with averaged grain orientations (Bohren & Huffman 1983). This means that infinitely long needles, for instance, are considered to be equally abundant as spheres or platelets. Such a quite extreme shape distribution could also give an estimate for the influence of grain aggregation (Huffman 1989, see also Stognienko et al. 1995; Michel et al. 1996). The calculation of the absorption spectra for such a CDE shows that it reproduces the measured band profile in position and width much better than the spectrum of spherical grains (see Fig.6).

The same is true for the bronzite as well as for the amorphous SiO_2 spheres (Fig.7). For the former, the morphological effects could also be responsible for a broadening and fusion of the indi-

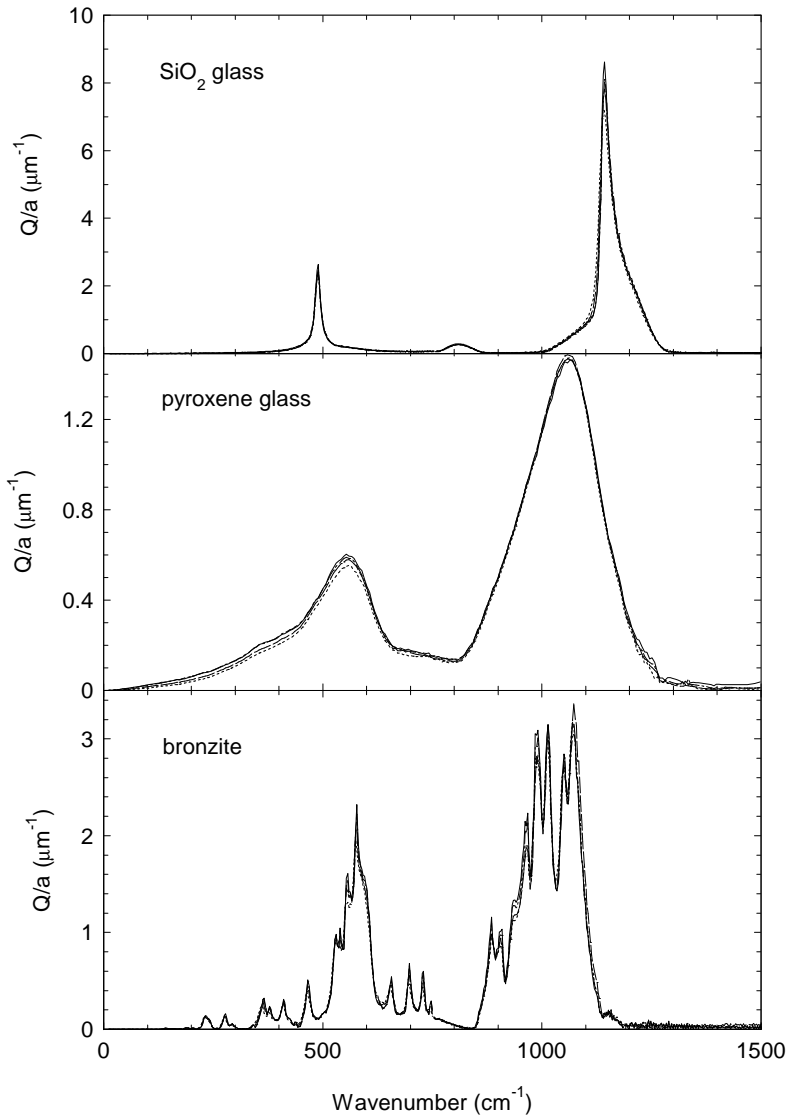


Fig. 3a. Absorption efficiency divided by particle radius calculated for spherical particles in vacuum from the optical data of Fig.2a. Temperatures: 300 K (dotted lines), 200 K (dashed lines), 100 K (dash-dotted lines), and 10 K (solid lines).

vidual features. However, one should also keep in mind that this material is polycrystalline and the averaging of the crystal axes may be incomplete in the reflectance and, therefore, in the calculated spectra. For the amorphous SiO_2 spheres, the discrepancy between the calculated and the measured band profiles is purely due to agglomeration. This has been proven by Schnaiter et al. (1996) by matrix-isolation spectroscopy. It has to be mentioned here that the additional band in the measured spectrum at about 950 cm^{-1} is due to hydroxyle impurities. For the “cosmic” pyroxene glass, the morphological effects are much weaker. The different band shape in the transmission spectrum in this case is obviously due to partial recrystallization of the powder sample.

5.2. Continuum FIR absorption

Apart from the temperature dependence of the bands and from the morphological effects discussed in the previous section, our interest in the transmission measurements originated mainly from the possible information about the continuous FIR absorp-

tion by disorder-induced, phonon-difference and free charge carrier processes. Such a continuum absorption is indeed observed in the transmission spectra of all materials. The Q/a values at selected wavelengths are given in Table 1. We generally give numbers with two significant digits because the relative error of the values produced by inhomogeneity of the pellets is about a few percent. For measured values smaller than $0.01 \mu\text{m}^{-1}$, however, one significant digit is sufficient because in that case the accuracy is limited by the sensitivity of the measurement to small absorptions.

For the sake of comparison, theoretical values for spherical and CDE particles embedded in PE have been calculated from the optical data of Fig.2b and have been included in Table 1. For the SiO_2 glass and the bronzite mineral, these values are very uncertain because for these materials the reflectance is too insensitive to the relatively small imaginary part of the refractive index. Consequently, no temperature or grain shape effect was detected in these calculations. However, for the bronzite there is a large discrepancy between the calculated (“reflection”) and

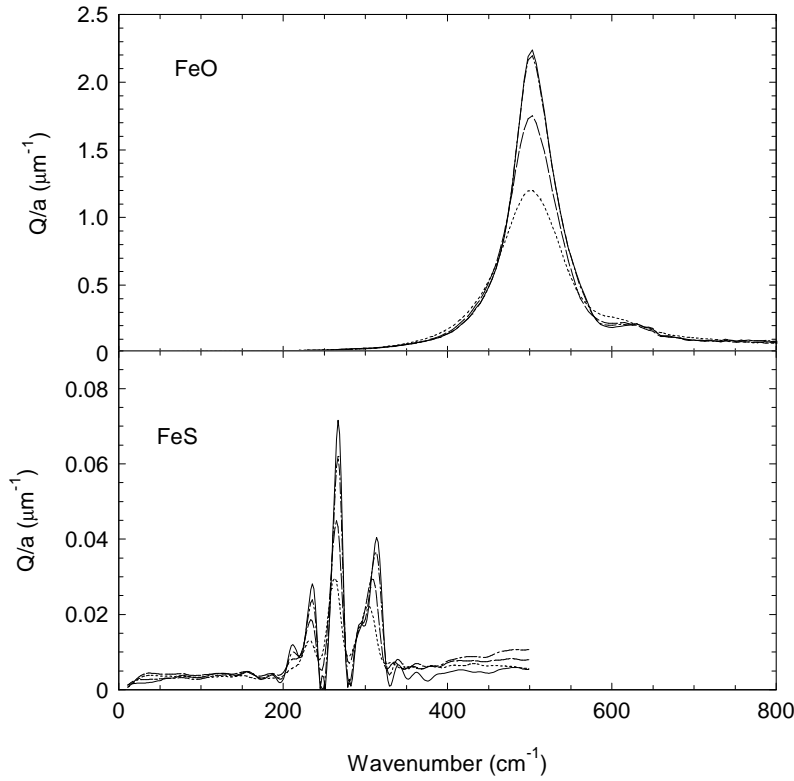


Fig. 3b. Absorption efficiency divided by particle radius calculated for spherical particles in vacuum from the optical data of Fig.2b. Temperatures: 300 K (dotted lines), 200 K (dashed lines), 100 K (dash-dotted lines), and 10 K (solid lines).

Table 1. Comparison of measured FIR small-particle absorption values (Q/a in μm^{-1}) with those calculated from the reflection data for Rayleigh spheres as well as for a continuous distribution of ellipsoids (CDE) embedded in polyethylene. The asterisk denotes very uncertain values which are only given for completeness (explanations see text).

wavelength		50 μm			100 μm			500 μm		
sample	T (K)	meas.	sphere	CDE	meas.	sphere	CDE	meas.	sphere	CDE
amorphous SiO ₂	300	0.050	0.02*	0.02*	0.029	0.005*	0.005*	0.009	$3 \cdot 10^{-4}$ *	$3 \cdot 10^{-4}$ *
	10	0.050	0.02*	0.02*	0.029	0.005*	0.005*	0.009	$3 \cdot 10^{-4}$ *	$3 \cdot 10^{-4}$ *
amorph. pyroxene	300	0.14	0.075	0.088	0.037	0.021	0.025	0.009	$9 \cdot 10^{-4}$	0.001
	10	0.14	0.12	0.14	0.037	0.051	0.062	0.009	0.004	0.005
bronzite	300	0.26	0.015*	0.015*	0.082	0.001*	0.001*	0.005	$5 \cdot 10^{-5}$ *	$5 \cdot 10^{-5}$ *
	10	0.21	0.015*	0.015*	0.055	0.001*	0.001*	0.005	$5 \cdot 10^{-5}$ *	$5 \cdot 10^{-5}$ *
FeO	300	0.28	0.051	0.14	0.21	0.038	0.095	0.083	0.010	0.041
	10	0.20	0.043	0.10	0.15	0.016	0.039	0.021	0.005	0.012
FeS	300	0.09	0.012	0.061	0.02	0.011	0.048	-	0.008	0.058
	10	0.09	0.012	0.052	0.02	0.011	0.047	-	0.005	0.022

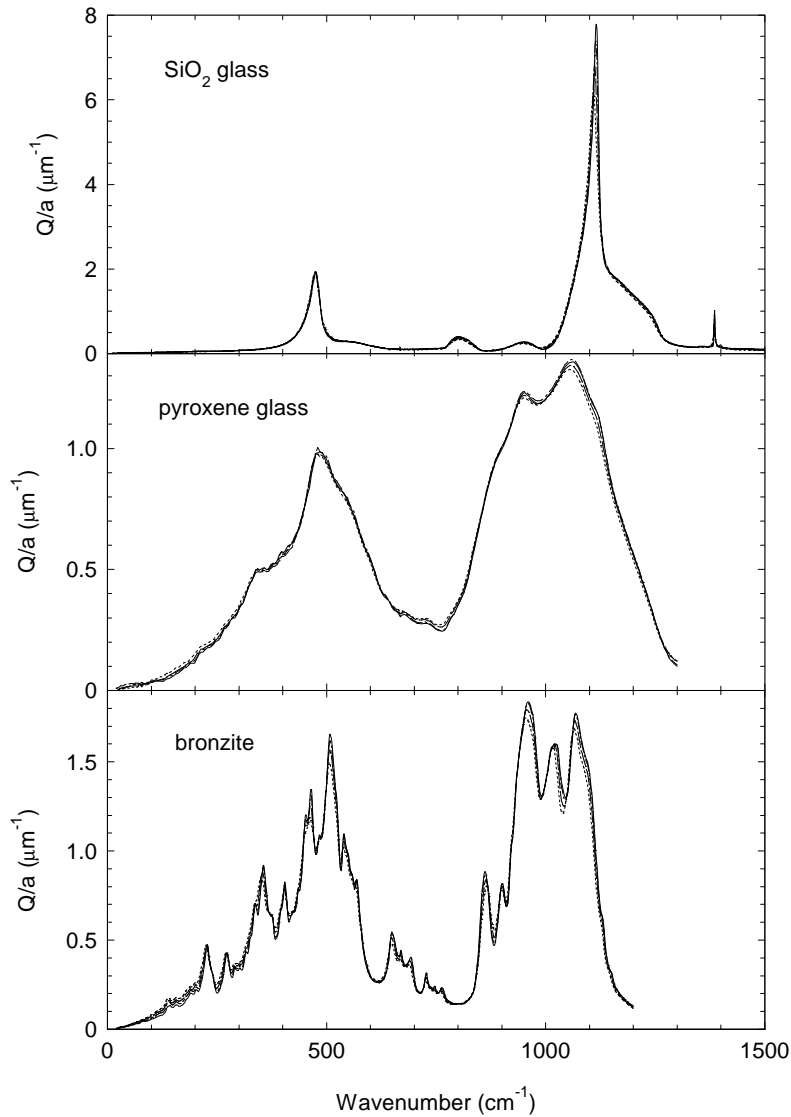


Fig. 4a. Measured absorption spectra of small silicate particles embedded in a transparent matrix (KBr, polyethylene). Temperatures: 300 K (dotted lines), 200 K (dashed lines), 100 K (dash-dotted lines), and 10 K (solid lines).

the measured (“transmission”) continuum absorptions. The reason for this could be amorphization of the material during the grinding process. This would enable disorder-induced single-phonon excitation to contribute to the absorption in the transmission spectra. This explanation is supported by the observed broadening of the vibrational bands in the bronzite transmission measurements. Nevertheless, there is a contribution from the phonon difference processes which can be identified in the transmission spectra by its temperature dependence.

The best agreement between the absorption values based on the transmission and reflection measurements is found in case of the amorphous silicates (with the above-mentioned reservations for the SiO_2 glass) for which the main contribution to the absorption is due to the disorder-induced single-phonon processes. In the transmission measurements, no temperature dependence has been found for both materials. In the calculated absorption of the “cosmic” silicate, however, the far-infrared transitions of the metal ions produce some small increase of the absorption with decreasing temperature. It is not clear, why this is not seen

in the transmission spectra. Possibly, it is masked by morphological effects. The absolute values at 20 cm^{-1} are comparable to those reported by Bösch (1978) and by Agladze et al. (1996) for soda-lime-silica glasses. The tunneling transitions studied in these papers, however, occur at wavenumbers downwards from 20 cm^{-1} so that a further comparison is not possible.

For the FeO and for the FeS, it is obvious that the CDE calculation matches the measured transmission values much better than the values calculated for spheres. This indicates that the strong FIR continuum measured probably is due to agglomeration. Aggregates of particles could form conducting paths which would efficiently increase the absorption cross section in the far infrared range (percolation) (see Henning & Stognienko 1995; Stognienko et al. 1995). The temperature dependence in the measured as well as in the calculated absorption values for both materials is not as large as expected. This may indicate that part of the free charge carriers in these materials is not thermally excited but due to impurities and defects in the crystal lattice.

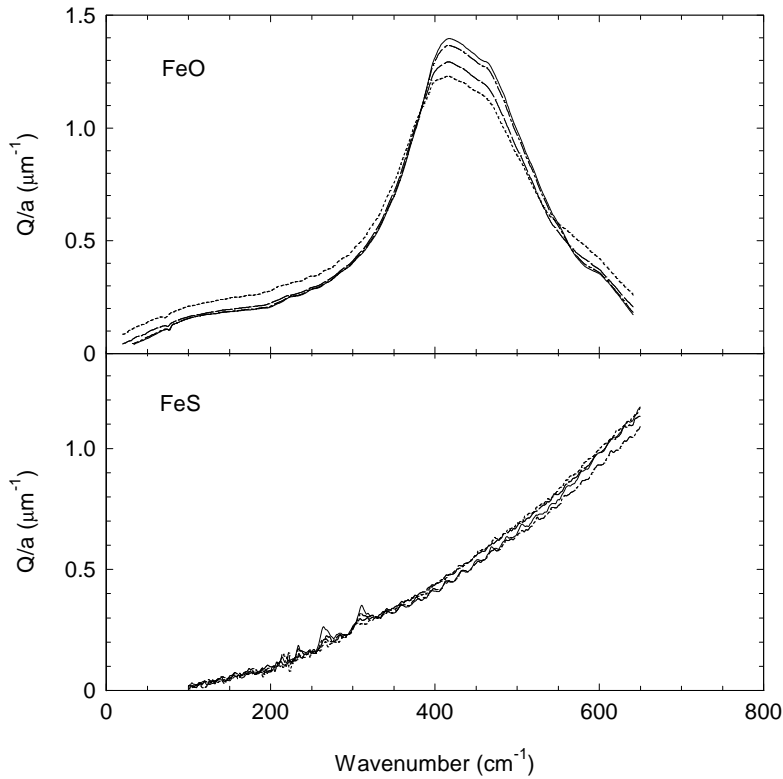


Fig. 4b. Measured absorption spectra of small iron compound particles embedded in a transparent matrix (KBr, polyethylene). Temperatures: 300 K (dotted lines), 200 K (dashed lines), 100 K (dash-dotted lines), and 10 K (solid lines).

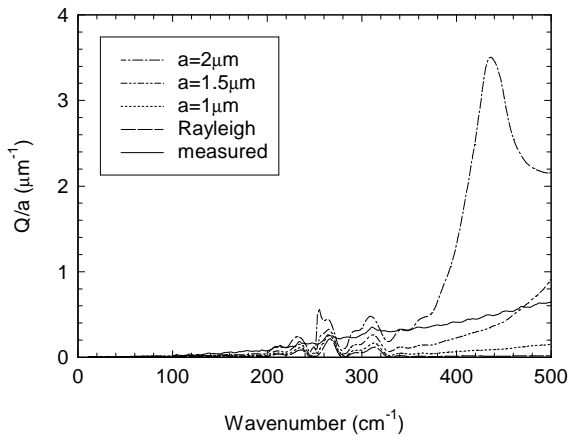


Fig. 5. Comparison of the measured FeS extinction spectrum (“transmission spectrum”) at 10 K with the calculated extinction (“reflection spectrum”) for spherical FeS grains of different sizes

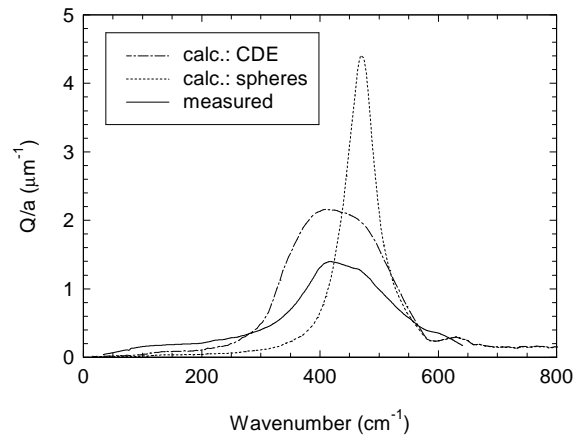


Fig. 6. Comparison of the measured FeO absorption spectrum (“transmission”) at 10 K with the calculated absorption (“reflection”) for FeO spheres and a CDE

6. Conclusion

The cosmic dust analogue materials investigated in this paper show sharpening and strengthening with decreasing temperature in their infrared vibrational bands which is generally important considering abundance constraints for solid materials in space. These effects are relatively strong (about a factor of two) for the iron compounds and surprisingly weak for crystalline silicates and quartz glass (about 10%). Especially, for the bronzite the strength of the 20 μm band increases much less with lowering

the temperature than it was reported by Day (1976) for a similar crystalline pyroxene (enstatite). For some of the bands the strengthening is connected with a shift towards shorter wavelengths which should one keep in mind when comparing interstellar and laboratory infrared band positions.

For a silicate glass of cosmic composition, there is no temperature dependence in the vibrational modes of the SiO_4 tetrahedra at about 10 and 20 μm wavelength but a strong temperature sensitivity was found for vibrational modes connected with metal ions, which occur at very large wavelengths. As

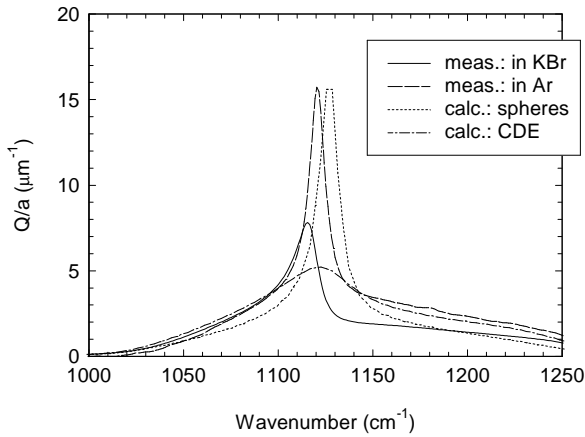


Fig. 7. Comparison of the measured SiO₂ absorption spectrum at 10 K (“transmission”) with the calculated absorption for SiO₂ spheres and a CDE (“reflection”) and with a measured absorption spectrum of SiO₂ spheres isolated in argon ice (from Schnaiter et al. 1996).

these transitions increase in strength with decreasing temperature they may be important to consider for the dense regions of the interstellar medium. This also holds for the continuum absorption processes operating at far-infrared wavelengths such as phonon-difference processes (e.g., in case of crystalline silicates) and free charge carrier absorption in semiconductors (e.g., in case of iron compounds), for which we found a decrease of absorption with falling temperature. This can be up to a factor of 4 at 500 μm in case of FeO. Such a change must be taken into account if physical parameters as the temperature and the mass are to be derived from measurements of the dust continuum radiation.

However, it came out in our measurements that both these effects can be masked by structural imperfections leading to disorder-induced single-phonon transitions and/or extrinsic charge carriers. This should be generally the case in cosmic grains. Therefore, both the temperature and the structure of the grains have to be taken into account when deriving reliable dust opacities for far-infrared wavelengths.

Detailed and quantitative studies of the continuum absorption at even longer wavelengths require transmission measurements of larger amounts of material which could be an important next step for future laboratory spectroscopy.

Acknowledgements. We wish to thank C. Jäger, B. Begemann, and J. Dorschner for the samples, G. Born for her preparational work and, especially, W. Teuschel for the construction of the cryo-setup and for the help with the measurements.

References

- Agladze N.I., Sievers A.J., Jones S.A., Burlitch J.M., Beckwith S.V.W. 1994, *Nature*, 372, 243
 Agladze N.I., Sievers A.J., Jones S.A., Burlitch J.M., Beckwith S.V.W. 1996, *ApJ*, 462, 1026

- Begemann B., Dorschner J., Henning Th., Mutschke H., Thamm E. 1994, *ApJ*, 423, L71
 Bohren C. F., Huffman D. R. 1983, *Absorption and Scattering of Light by Small Particles*, John Wiley, New York
 Bösch M.A. 1978, *Phys. Rev. Lett.*, 40(13), 879
 Day K.L. 1976, *ApJ*, 203, L99
 Dorschner J., Begemann B., Henning Th., Jäger C., Mutschke H. 1995, *A&A*, 300, 503
 Dorschner J., Friedemann C., Gürtler J., Henning Th. 1988, *A&A*, 198, 223
 Dorschner J., Gürtler J., Henning Th. 1989, *Astron. Nachr.*, 310, 303
 Gervais F., Blin A., Massiot D., et al. 1987, *J. Non-Cryst. Sol.*, 89, 384
 Hadni A. 1970, in S. S. Mitra and S. Nudelman (eds.), *Far-Infrared Properties of Solids*, Plenum Press, New York, pp 561–587
 Harbecke B. 1986, *Appl. Phys. A*, 40, 151
 Henning Th., Michel B., Stognienko R. 1995a, *Planet. Space Sci.*, 43, 1333
 Henning Th., Begemann B., Dorschner J., Mutschke H. 1995b, *A&AS*, 112, 143
 Henning Th., Stognienko R. 1995, *A&A*, 311, 291
 Huffman D.R. 1989, in A. G. G. M. Tielens and L. J. Allamandola (eds.), *Interstellar Dust*, Proc. of IAU Symposium 135, Kluwer, Dordrecht, p.329
 Jäger C. 1997, Ph.D. thesis, Univ. Jena
 Jäger C., Mutschke H., Begemann B., Dorschner J., Henning Th. 1994, *A&A*, 292, 641
 Jasperse J.R., Kahan A., Plendl J.N., Mitra S.S. 1966, *Phys. Rev.*, 146, 526
 Michel B., Henning Th., Stognienko R., Rouleau F. 1996, *ApJ*, 468, 834
 Mon K.K., Chabal Y.J., Sievers A.J. 1975, *Phys. Rev. Lett.*, 35(20), 1352
 Mutschke H., Begemann B., Dorschner J., Henning Th. 1994, *Infrared Phys. Technol.*, 35, 361
 Schnaiter M., Henning Th., Mutschke H. 1996, in J. P. Maier and M. Quack (eds.), *Proc. SASP 96*, VdF, Zürich, p. 246
 Seki J., Yamamoto T. 1980, *Ap&SS*, 72, 79
 Stognienko R., Henning Th., Ossenkopf V. 1995, *A&A*, 296, 797
 Stolen R., Dransfeld K. 1965, *Phys. Rev.*, 139, A1295
 Strom U., Taylor P.C. 1977, *Phys. Rev. B*, 16(12), 5512
 Waters L.B.F.M., Molster F.J., de Jong T., et al. 1996, *A&A*, 315, L361
 Yu P.Y., Cardona M. 1996, *Fundamentals of Semiconductors*, Chapt. 6.2, Springer, Berlin